Supporting Information

The stability landscape of *de novo* TIM barrels explored by a modular design approach

Sergio Romero-Romero, Miguel Costas, Daniel-Adriano Silva Manzano, Sina Kordes, Erendira Rojas-Ortega, Cinthya Tapia, Yasel Guerra, Sooruban Shanmugaratnam, Adela Rodríguez-Romero, David Baker,* Birte Höcker,* D. Alejandro Fernández-Velasco.*

* Corresponding authors. D. A. Fernández-Velasco: fdaniel@unam.mx, B. Höcker: birte.hoecker@uni-bayreuth.de, D. Baker: dabaker@uw.edu

This file includes:

- Supporting Text.
- Supplementary Figures S1 to S15.
- Supplementary Tables S1 to S7.

Supporting Text

Exploratory characterization of first-round designs

The proteins from the first design round (DeNovoTIMs 1-10) as well as DeNovoTIM0, sTIM11, and sTIM11noCys were characterized by circular dichroism (CD) and differential scanning calorimetry (DSC) (Fig. S3). All variants presented far-UV CD spectra with a high content of regular secondary structural elements compatible with α/β proteins. For sTIM11 and sTIM11noCys, the most pronounced minimum of the spectra was observed at 222 nm whereas, for DeNovoTIM0 and DeNovoTIM1-10, it was found at 206 and 208 nm, respectively (Fig. S3 and Fig. S4A). According to the Gibbs Helmholtz equation, high T_m and ΔH values are reflected in larger areas under the stability curve, therefore, selection of the best designs was based on their thermal unfolding parameters.

Analysis of the internal core designs showed that DeNovoTIM2 and DeNovoTIM3 unfold irreversibly and uncooperatively, whereas DeNovoTIM4 unfolds cooperatively with a T_m value which is 15 degrees higher than DeNovoTIM0 (Fig. S3B). However, DeNovoTIM1 unfolds cooperatively with a further increased T_m that is 24 degrees higher than DeNovoTIM0 (Fig. S3B) and its unfolding ΔH determined by the DSC endotherm is almost twice than that of DeNovoTIM0 (Fig. S3C). Thus, DeNovoTIM1 was chosen as the best design of this group. Amongst the bottom core

designs, DeNovoTIM7 did not overexpress soluble, and no significant efforts were made to solubilize it after unfolding/refolding of inclusion bodies. The thermal unfolding of DeNovoTIM5 is less cooperative and the protein unfolds with a T_m slightly higher than DeNovoTIM0. In contrast, DeNovoTIM6 has a T_m that is 45 degrees higher than DeNovoTIM0 and shows a highly cooperative unfolding transition (Fig. S3E-S3F and table 1). Hence, DeNovoTIM6 is the most successful design within this group. Finally, all top core designs (DeNovoTIM8-10) unfold cooperatively; nevertheless, DeNovoTIM8 displays the highest T_m and ΔH of this group (Fig. S3H-S3I). Therefore, DeNovoTIM8 is considered the best design among the proteins belonging to this group.

Spectroscopic and hydrodynamic characterization of DeNovoTIMs

sTIM11, sTIM11noCys, and all DeNovoTIM variants presented the characteristic far-UV CD spectra observed for α/β proteins (Fig. 2A). Nevertheless, the secondary structure content deconvoluted from the spectra showed variations in the relative amount of helices and strands, particularly for DeNovoTIM0 and DeNovoTIM1, which have the lowest helical content (table S5). For those DeNovoTIMs for which a three-dimensional structure was obtained (see below), the secondary structure content calculated from the structure and the deconvolution of CD spectra correlates adequately (table S5).

The near-UV CD spectra of DeNovoTIMs (Fig. 2B) showed a peak with fine structure between 290 and 295 nm, characteristic for tryptophan residues. A peak between 275-283 nm was also observed in the designs that contain tyrosine residues (table S3). It is known that the shape and intensities of the near-UV CD spectrum depend not only on the number and identity of aromatic residues but also on their environment and three-dimensional position within the protein core [89]. The spectra observed in Fig. 2B indicate that aromatic residues in the protein are structured with significant differences in the native environment. The latter is in agreement with the intrinsic fluorescence (IF) spectra, where native λ_{max} is in the 329-345 nm range (Fig. 2C and Fig. S6). Likewise, the spectral center of mass (SCM) is between 346 and 357 nm, indicating differences in the environment of aromatic residues among native DeNovoTIMs (table S5). The fluorescence properties of DeNovoTIM0 indicate partial exposure of aromatic residues. All first-round designs show a considerable blue-shift in both λ_{max} and SCM; this trend continues in the second- and third-round designs and should be attributed to changes in both the number and the solvent exposure of Trp residues (table S3 and table S5).

All DeNovoTIMs adopt a monomeric and compact shape as revealed by the invariant value of the Stokes radius determined by analytical size exclusion chromatography over a twenty-fold protein concentration range (table S5). DeNovoTIM0 is also monomeric but shows a Stokes radius (26.1 ± 0.3 Å) slightly higher than that expected for a compact protein of this size (22.5 ± 1.0 Å), but still far

away from the expected value for an unfolded conformation (42.0 ± 1.0 Å) [33]. This is in agreement with the red shift in the IF spectra and suggests a slightly expanded conformation for DeNovoTIM0.

Residual structure in the thermal unfolding of DeNovoTIMs

All DeNovoTIMs, except DeNovoTIM13 and DeNovoTIM14, showed reversibility i.e. samples were heated up to 125 °C and their endotherms were completely recovered in a second heating scan (Fig. S7). All reversible transitions were well fitted to the two-state model (N⇋U) (Fig. S8) and the calorimetric criterion ($\Delta H_{vH}/\Delta H$) was very close to 1, in agreement with a two-state mechanism (table 1). DSC experiments performed at different protein concentrations (0.25 to 2.5 mg mL^{-1}) exhibited the same T_m, indicating that thermal unfolding is under thermodynamic control (Fig. S8).

The observed unfolding ΔH varies greatly, showing values both lower and higher than DeNovoTIM0, sTIM11noCys, and sTIM11 (table 1). When proteins of the same size are compared, the main reasons for finding differences in their unfolding ΔH are the number of disrupted internal interactions, as well as the hydration of groups exposed upon unfolding [90]. Extreme scenarios were observed in DeNovoTIMs, e.g. DeNovoTIM6 has a ΔH= 125 ± 2 kcal mol^{-1}, which is 100 kcal mol^{-1} more than that of DeNovoTIM0, and close to the expected value for a protein of 184 residues according to previously reported parametric equations (128 ± 4 kcal mol^{-1}) [34].

Otherwise, several DeNovoTIMs exhibit small ΔH values, particularly DeNovoTIM14 (ΔH= 14 kcal mol^{-1}; Fig. S10E and table 1). There are at least two main reasons for such a small ΔH, namely either the native state is not fully folded or the unfolded state is not completely unfolded. The spectroscopic, structural, and chemical unfolding properties shown in Fig. 2 indicate that the proteins are well folded in the native state, a conclusion that is supported by the crystal structures (see below). It is known that both ΔH and T_m decrease in the presence of chemical denaturants [91]. When DeNovoTIM14 was unfolded by temperature in the presence of urea, the second transition disappeared and the T_m of the observed endotherm remained almost unchanged at ~90 °C (Fig. 2F, Fig. S10B, and Fig. S10D). Unexpectedly, the unfolding enthalpy increased linearly from the value observed without denaturant to a value close to the parametric one at 6.0 M urea (Fig. S10A and Fig. S10E). This atypical behavior in DeNovoTIM14 may be explained by an increased exposure of nonpolar residues upon unfolding in the presence of urea. These results suggest that the reason for the low unfolding enthalpy in some DeNovoTIMs is likely the high content of residual structure in the unfolded state.

Likewise, it has been shown that the residual structure of the unfolded state leads to decreased ΔC_P values [35]. For sTIM11, sTIM11noCys, and DeNovoTIM6, the ΔC_P were close to the estimated value from parametric equations for a protein of that size (2.6 kcal mol^{-1} K^{-1}), whereas the other DeNovoTIMs showed a much lower ΔC_P, with DeNovoTIM0 having the lowest value (0.44 kcal mol^{-1} K^{-1}, table 1). Accuracy in

thermodynamic parameters of unfolding has been discussed over the years and is especially crucial for ΔC_P due to the baseline shift and its small magnitude. For DeNovoTIMs, the obtention of ΔC_P was addressed with multiple determinations at varying protein concentration. The standard deviation ranged from 3 to 20 %, very similar to previous estimates for uncertainties in ΔC_P [34,3]. A decrease in unfolding ΔC_P suggests a non-fully solvated random-coil conformation with residual hydrophobic clusters in the unfolded state. Even though it was not possible to obtain the CD spectra of DeNovoTIMs that display T_m values higher than 90 °C, CD spectra of the unfolded state of the low T_m variants DeNovoTIM0, DeNovoTIM1, and DeNovoTIM8, as well as sTIM11 and sTIM11noCys, clearly showed residual structure (Fig. S4B).

Irreversible thermal unfolding of DeNovoTIM13 and DeNovoTIM14

DeNovoTIM13 shows a T_m scan-rate dependent, indicating that its thermal unfolding is under kinetic control (Fig. S9). Because the irreversible thermal unfolding of DeNovoTIM13 and DeNovoTIM14 follows an irreversible two-state mechanism (N→F), well described by a first-order rate constant [74,75], it was possible to determine the activation energy (E_{act}) between the native and the transition state. For DeNovoTIM13, the average value obtained from the fitting of each endotherm (E_{act}= 118.2 ± 2.7 kcal mol^{-1}; Fig. S9A) is within the range reported for natural proteins of similar size. This value agrees with that determined from the Arrhenius plot (E_{act}= 118 ± 2 kcal mol^{-1}; Fig. S9B) and with the calculation from the effect of the scan rate on T_m (E_{act}= 124 ± 2 kcal

mol^{-1}; Fig. S9C).

In contrast, for DeNovoTIM14 a much lower kinetic stability was observed fitting the endotherms to the irreversible two-state model (E_{act}= 38 ± 1 kcal mol^{-1}; Fig. S10A), determined from the Arrhenius plot (E_{act}= 38 ± 1 kcal mol^{-1}; Fig. S10C), and extrapolating to 0 M urea (E_{act}= 37 ± 1 kcal mol^{-1}; Fig. S10F). As a consequence of having very different kinetic stabilities, the estimated half-life of DeNovoTIM13 at 25 °C is 1.8 x 10^{10} years and about 196 days for DeNovoTIM14. Clearly, it would be interesting to determine folding/unfolding rates in future kinetic studies of the *de novo* designed TIM barrels.

Supplementary Figures

List of supplementary figures

- Fig. S1: Flowchart of the Rosetta design protocol used to generate the DeNovoTIM collection.
- Fig. S2: Sequence alignment of DeNovoTIM barrels.
- Fig. S3: Exploratory characterization of first-round designs.
- Fig. S4: CD spectra in the peptidic region for DeNovoTIMs.
- Fig. S5: CD spectra in the aromatic region for DeNovoTIMs.
- Fig. S6: Intrinsic fluorescence spectra of DeNovoTIMs.
- Fig. S7: DSC instrument equilibration and thermal unfolding reversibility assessment of DeNovoTIMs.
- Fig. S8: DSC endotherms of DeNovoTIMs.
- Fig. S9: Irreversible thermal unfolding of DeNovoTIM13.
- Fig. S10: Irreversible thermal unfolding of DeNovoTIM14 in the presence of urea.
- Fig. S11: ΔC_P determination of DeNovoTIMs at different protein concentrations.
- Fig. S12: Chemical unfolding of DeNovoTIMs followed by CD and IF (raw data).
- Fig. S13: Chemical unfolding of DeNovoTIMs followed by CD and IF (normalized data).
- Fig. S14: Thermodynamic cycles for DeNovoTIMs.
- Fig. S15: Hydrophobic clusters of DeNovoTIMs.

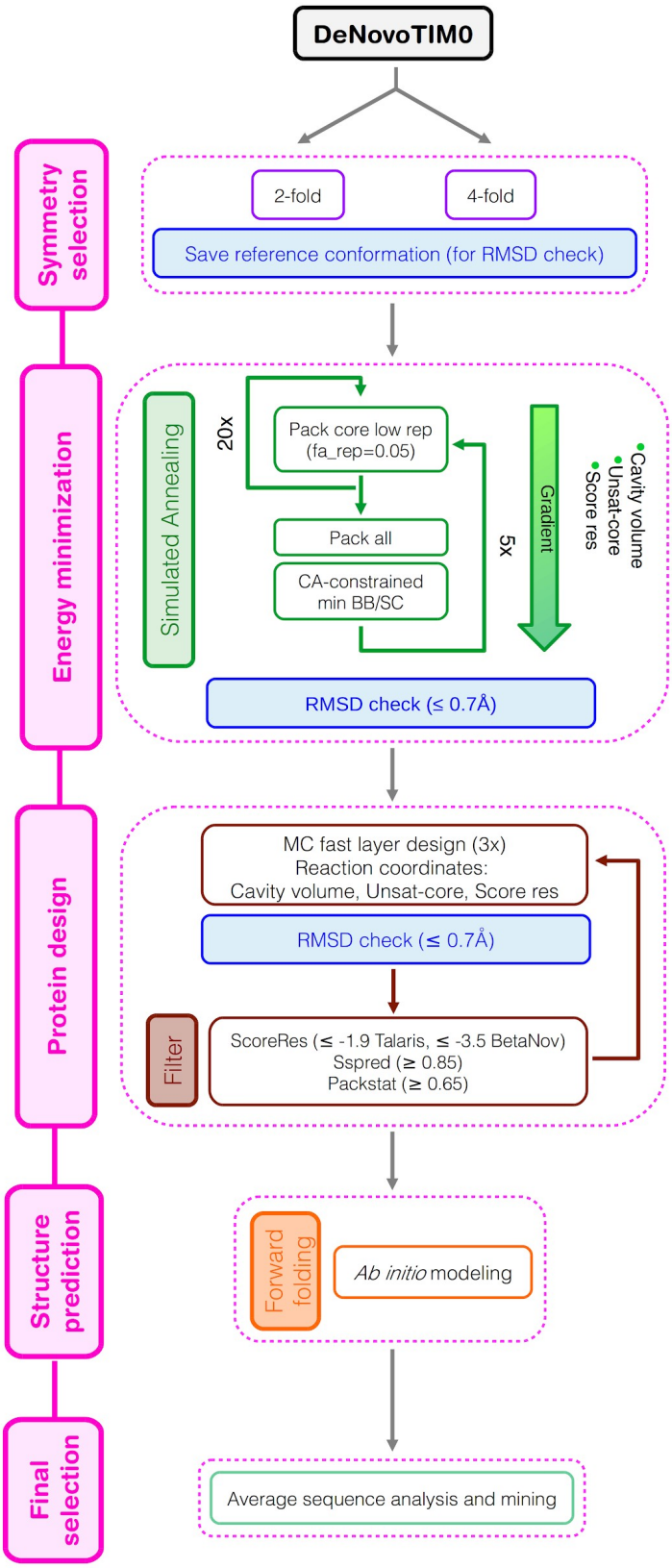

Fig. S1. Flowchart of the Rosetta design protocol used to generate the DeNovoTIM collection.

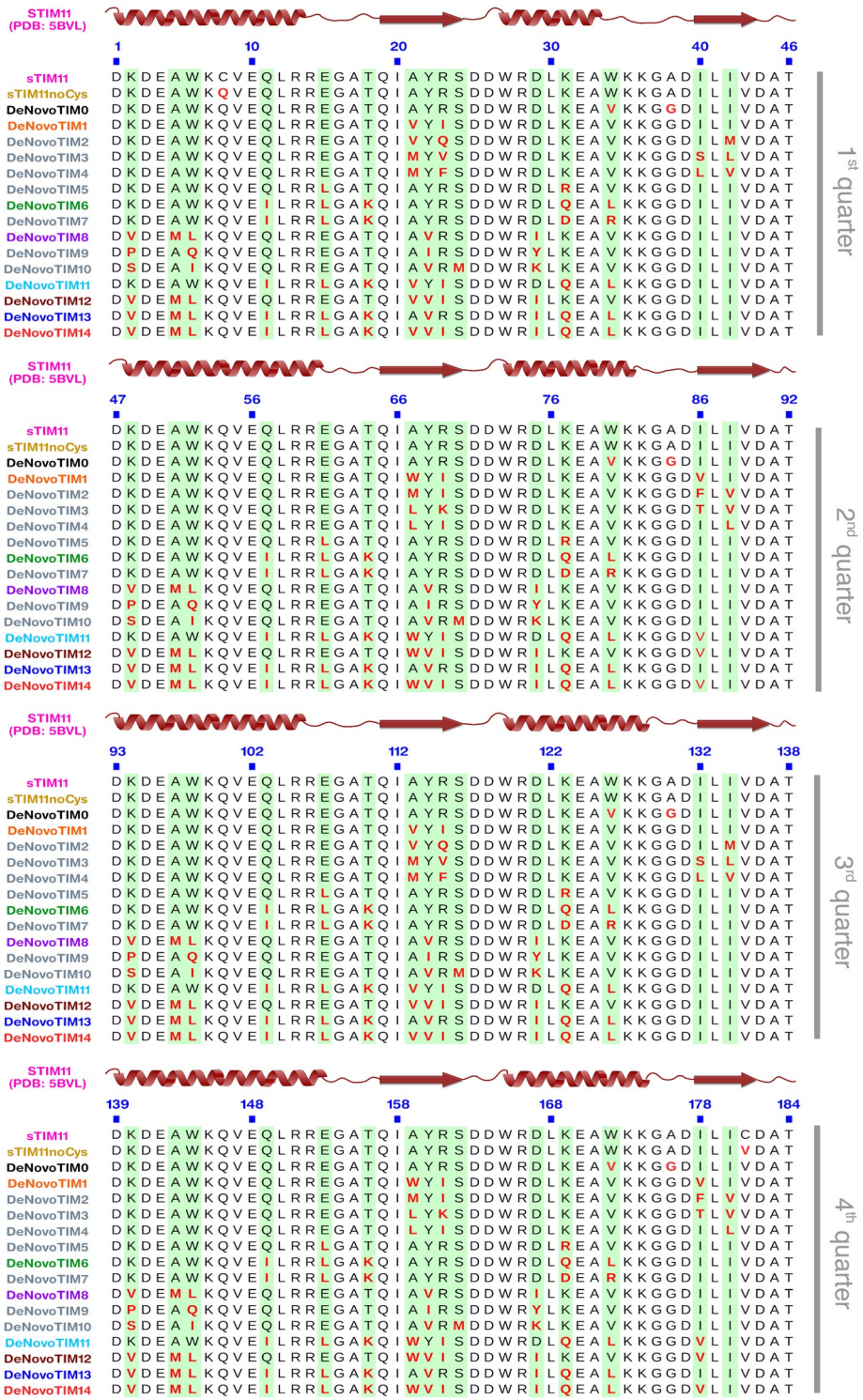

Fig. S2. Sequence alignment of DeNovoTIM barrels. On top of each TIM barrel quarter, the secondary structure of sTIM11 is shown (PDB ID: 5BVL). Mutations incorporated in each design are highlighted in red. sTIM11noCys is the symmetric version of sTIM11 removing the cysteine residues (C8Q/C181V). DeNovoTIM0 contains the additional mutations W34V and A38G, as well as their symmetry-related positions. See table S2 for a complete list of the mutations.

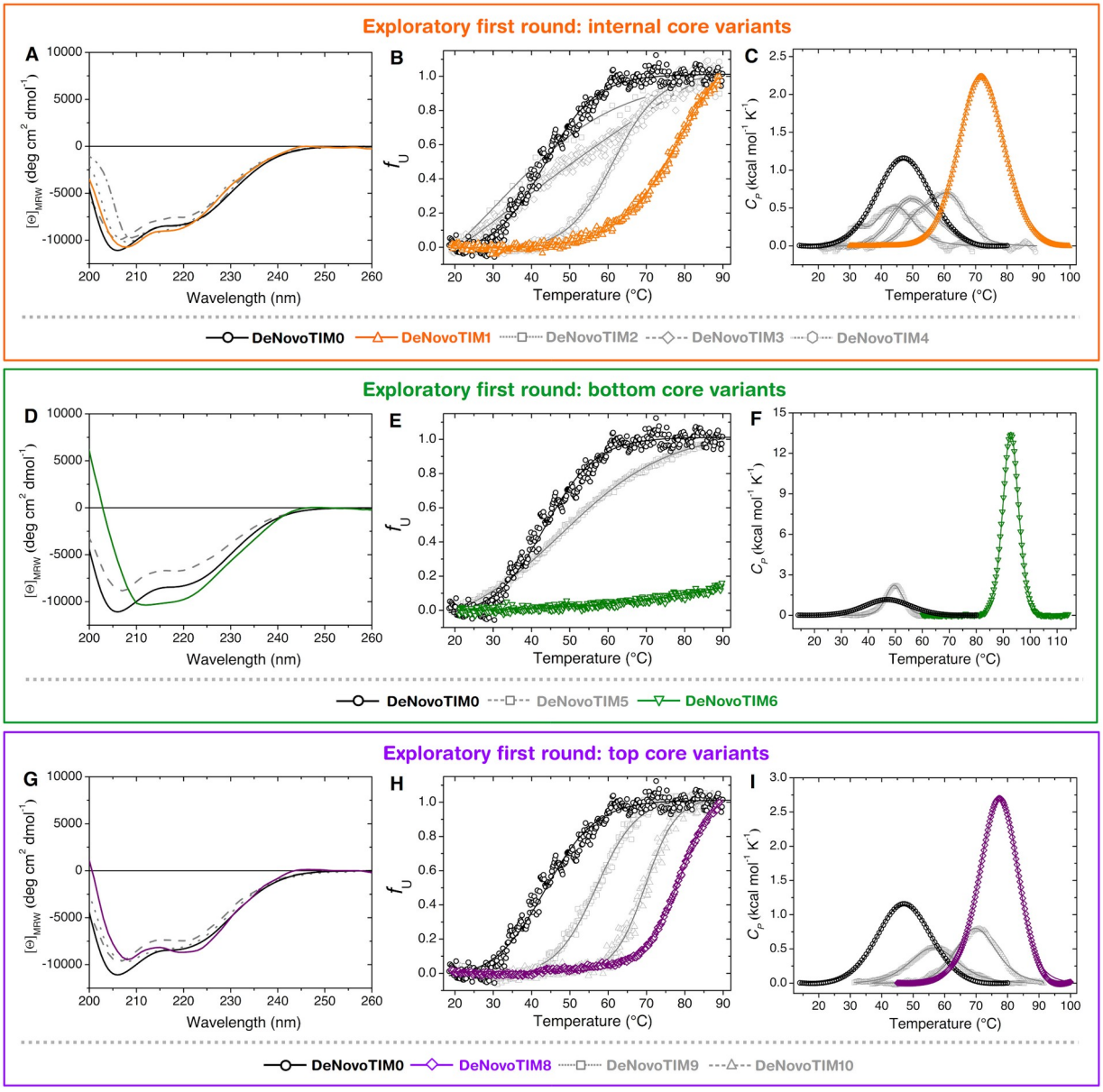

Fig. S3. Exploratory characterization of first-round designs. Far-UV CD spectra are shown in panels **A**, **D**, and **G**. Normalized thermal unfolding data followed by $CD_{222\ nm}$ are presented in panels **B**, **E**, and **H**. Thermal unfolding experiments followed by DSC are shown in panels **C**, **F**, and **I**. Selected variants of each design group are highlighted in orange (DeNovoTIM1), green (DeNovoTIM6), or purple (DeNovoTIM8). In all experiments protein concentration was 0.4 mg mL^{-1} in 10 mM sodium phosphate pH 8.

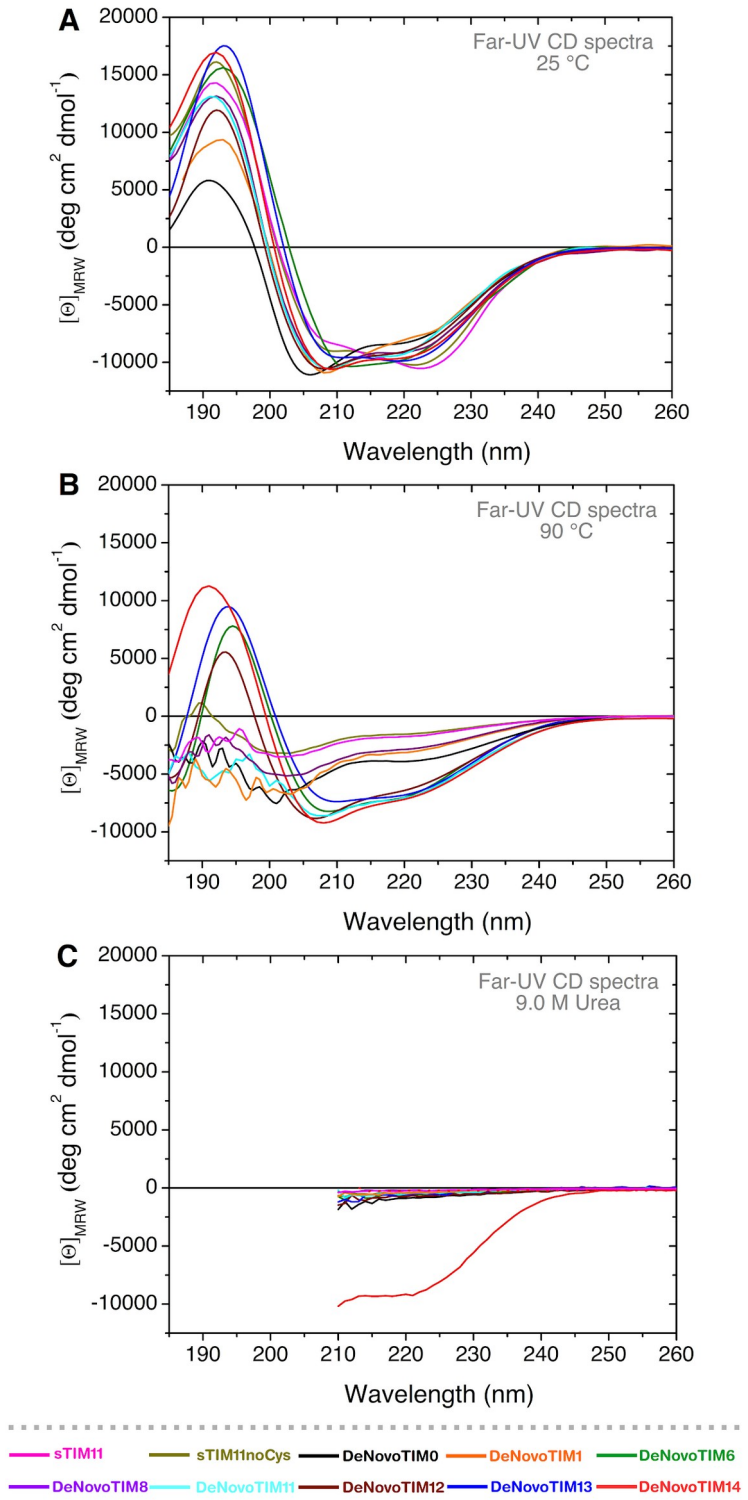

Fig. S4. CD spectra in the peptidic region for DeNovoTIMs. Far-UV CD spectra at 25 °C **(A)**, 90 °C **(B)**, and 9.0 M urea **(C)**. Note that for DeNovoTIM14 at 9.0 M urea (solid red line) the spectrum is very similar to the native one (panel **A**). In 7.0 M GdnHCl the protein is completely unfolded and its spectrum is identical to all other DeNovoTIMs unfolded in 9.0 M urea (dotted red line). In all experiments protein concentration was 0.4 mg mL^{-1} in 10 mM sodium phosphate pH 8.

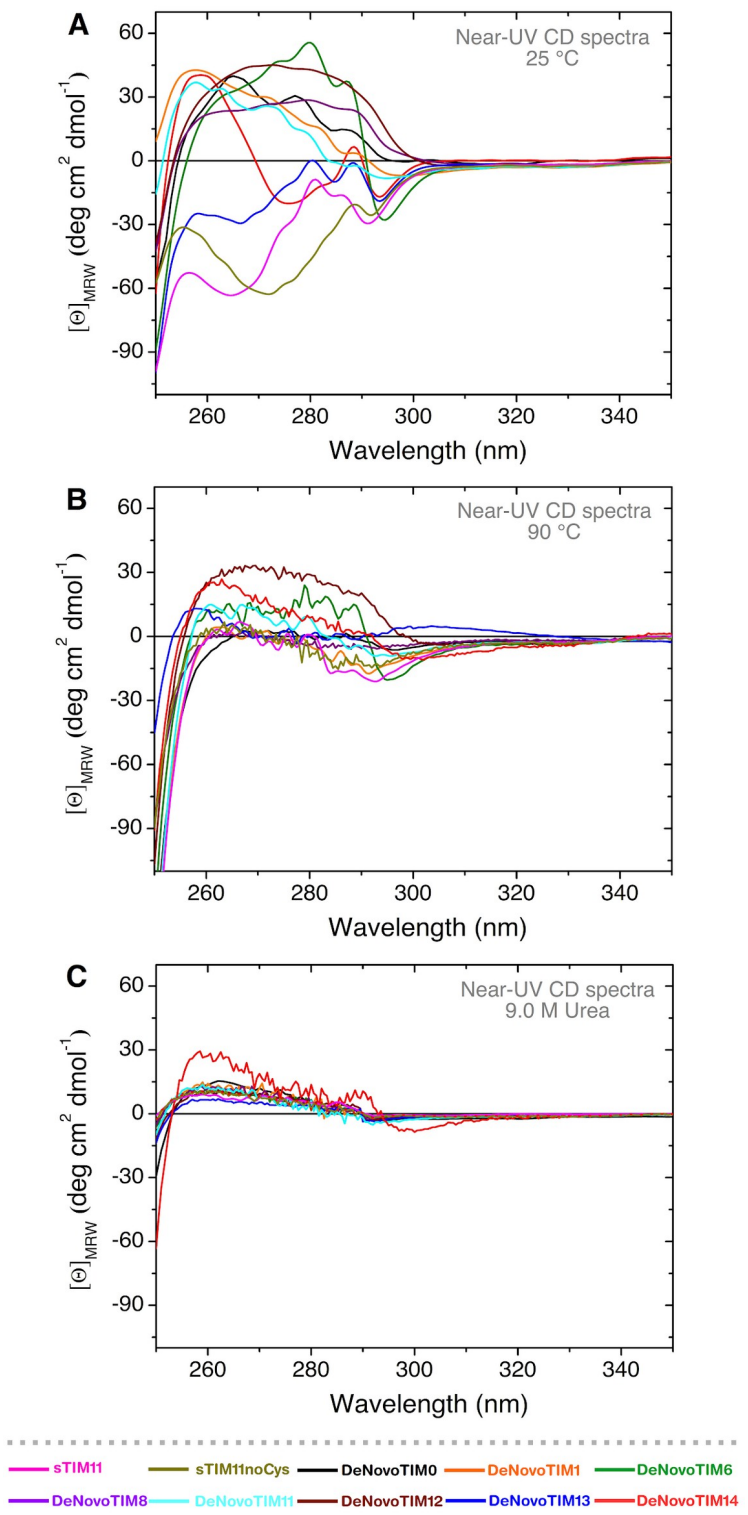

Fig. S5. CD spectra in the aromatic region for DeNovoTIMs. Near-UV CD spectra at 25 °C **(A)**, 90 °C **(B)**, and 9.0 M urea **(C)**. Note that for DeNovoTIM14 at 9.0 M urea (solid red line) the spectrum is very similar to the native one (panel **A**). In 7.0 M GdnHCl the protein is completely unfolded and its spectrum is identical to all other DeNovoTIMs unfolded in 9.0 M urea (dotted red line). In all experiments protein concentration was 0.4 mg mL^{-1} in 10 mM sodium phosphate pH 8.

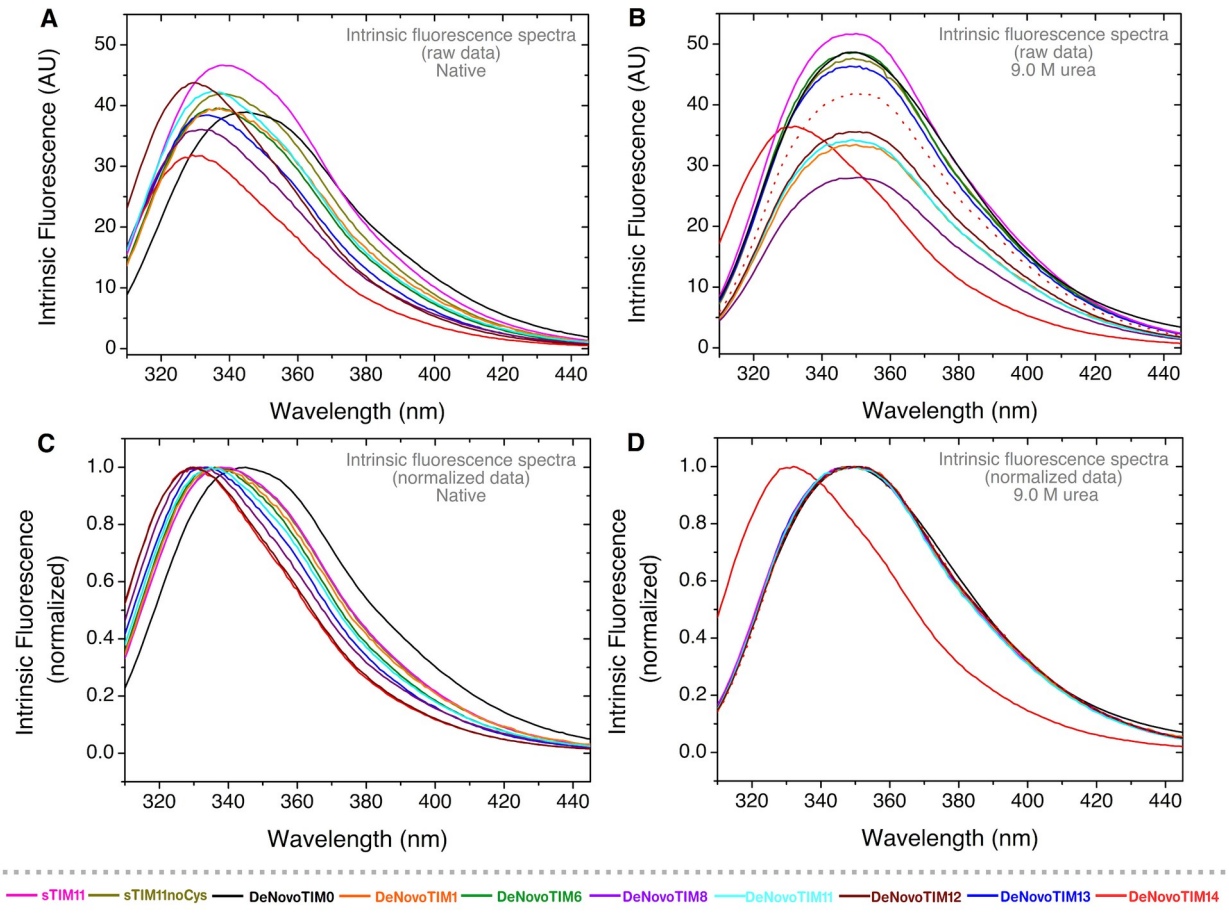

Fig. S6. Intrinsic fluorescence spectra of DeNovoTIMs. Native spectra are presented in panel **A** (raw data) and **C** (normalized data). Spectra obtained in 9.0 M urea are presented in panel **B** (raw data) and **D** (normalized data). Note that for DeNovoTIM14 in 9.0 M urea (solid red lines in panels **B** and **D**) the spectra are very similar to the native ones (solid red lines in panels **A** and **C**). In 7.0 M GdnHCl the protein is completely unfolded and its spectrum is identical to all other DeNovoTIMs unfolded in urea (dotted red line in panels **C** and **D**). In all experiments protein concentration was 0.4 mg mL^{-1} in 10 mM sodium phosphate pH 8.

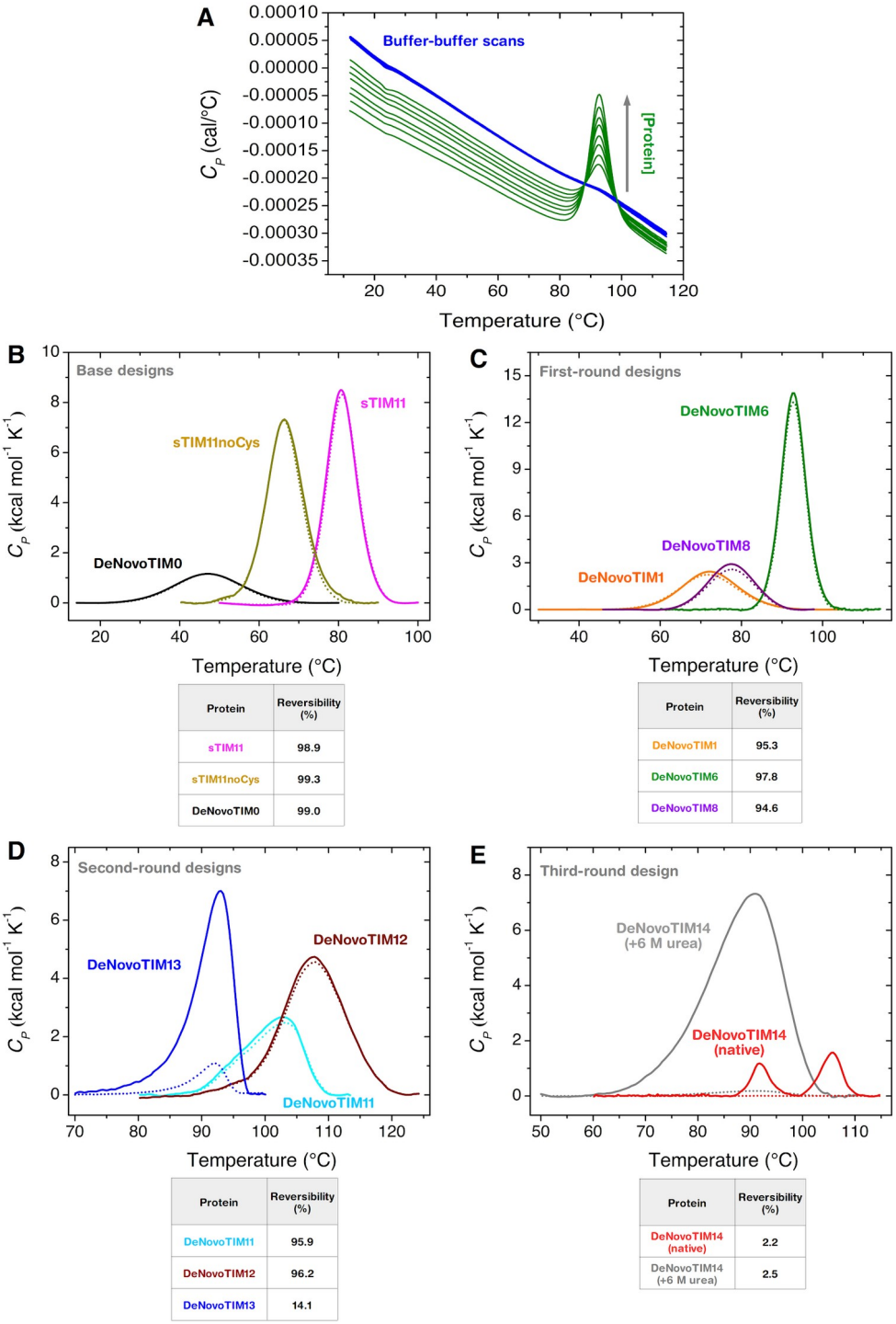

Protein	Reversibility (%)
sTIM11	98.9
sTIM11noCys	99.3
DeNovoTIM0	99.0

Protein	Reversibility (%)
DeNovoTIM1	95.3
DeNovoTIM6	97.8
DeNovoTIM8	94.6

Protein	Reversibility (%)
DeNovoTIM11	95.9
DeNovoTIM12	96.2
DeNovoTIM13	14.1

Protein	Reversibility (%)
DeNovoTIM14 (native)	2.2
DeNovoTIM14 (+6 M urea)	2.5

Fig. S7. DSC instrument equilibration and thermal unfolding reversibility assessment of DeNovoTIMs. **A)** Proper instrument equilibration was ascertained by performing two buffer-buffer scans before each protein-buffer scan. One example at different protein concentrations (DeNovoTIM6) is shown in the panel. **B-E)** Thermal unfolding reversibility was assessed with 1.0 mg protein mL^{-1} and 1 K min^{-1} in 10 mM sodium phosphate pH 8. Continuous lines show the first scan and dotted lines show the second scan collected after cooling down and reheating the sample. Reversibility % was calculated as the ratio of the calorimetric ΔH (area under the curve) recovered in the second scan and that obtained in the first scan ($\Delta H_{\text{secondscan}}/\Delta H_{\text{firstscan}}$)*100.

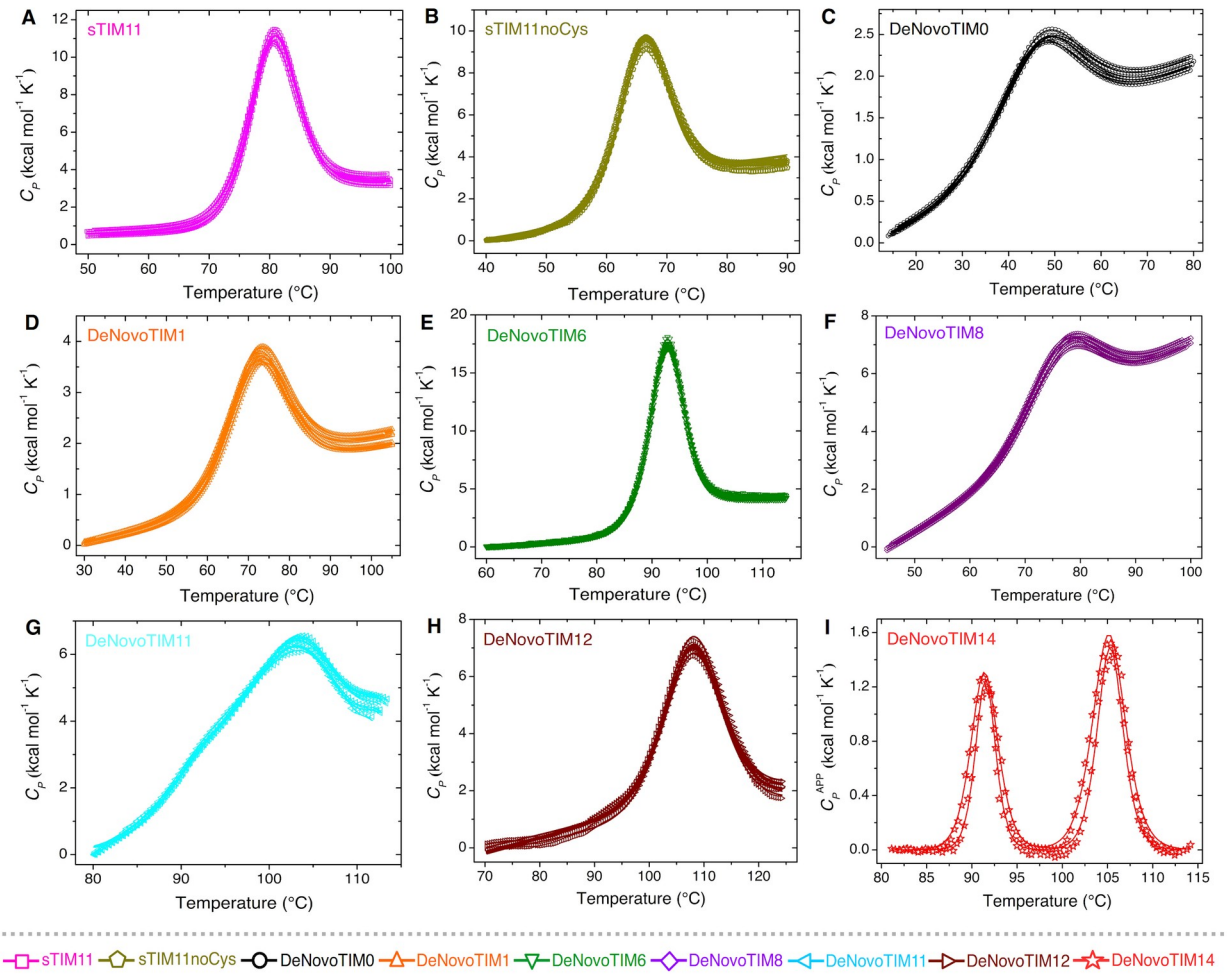

Fig. S8. DSC endotherms of DeNovoTIMs. Experiments were carried out at different protein concentrations (panels **A-H**: 0.25-2.5 mg mL^{-1}, panel **I**: 2.5 and 4.5 mg mL^{-1}). Open symbols show experimental data and solid lines are the best fits to a two-state model, except for DeNovoTIM14 where a non-two-state model with two transitions was used.

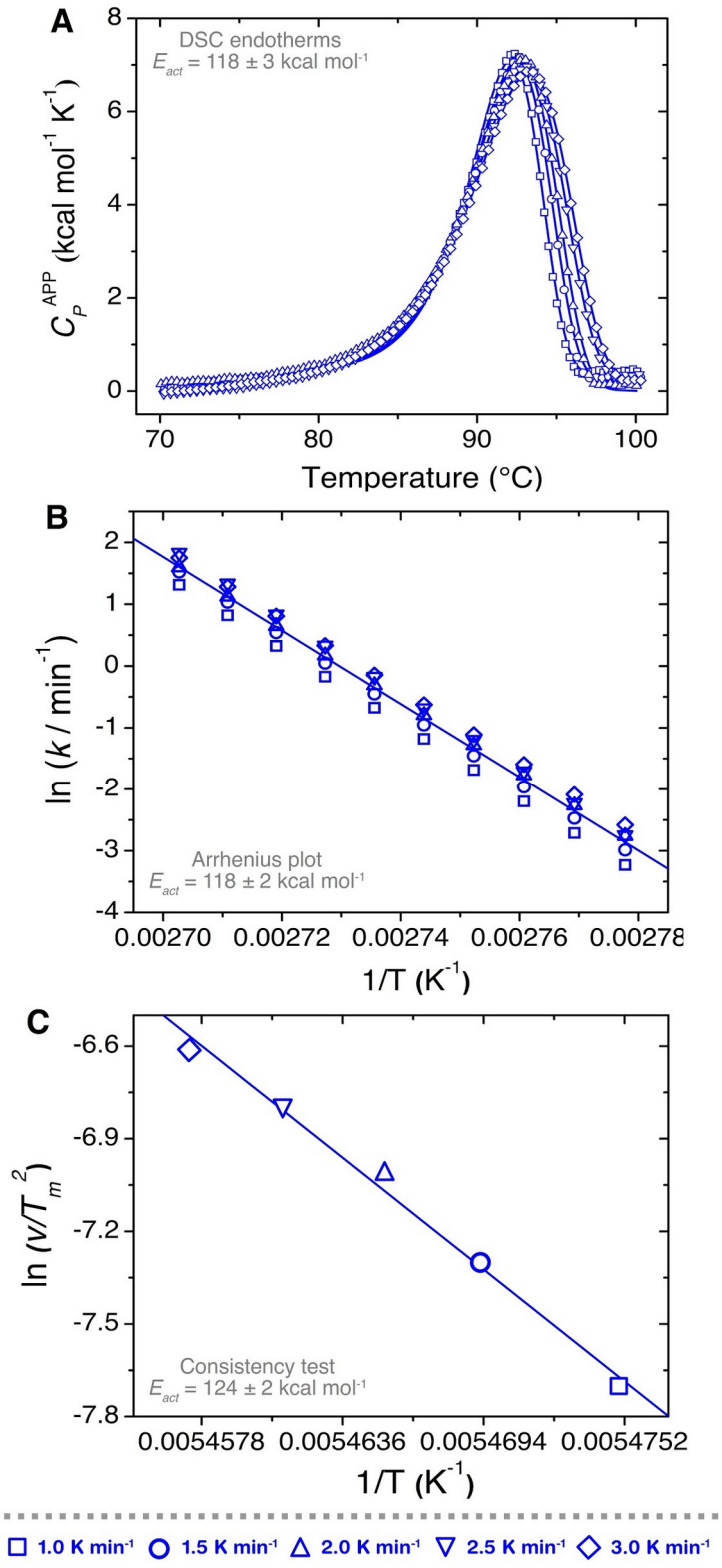

Fig. S9. Irreversible thermal unfolding of DeNovoTIM13. A) Endotherms at different scan rates (1 to 3 K min^{-1}). Lines represent the best fit to a two-state irreversible model. **B)** Arrhenius plot. The line shows the best fit to the Arrhenius equation (R^2: 0.98). **C)** Effect of the scan rate on T_m (R^2: 0.99). In all experiments protein concentration was 0.5 mg mL^{-1} in 10 mM sodium phosphate pH 8.

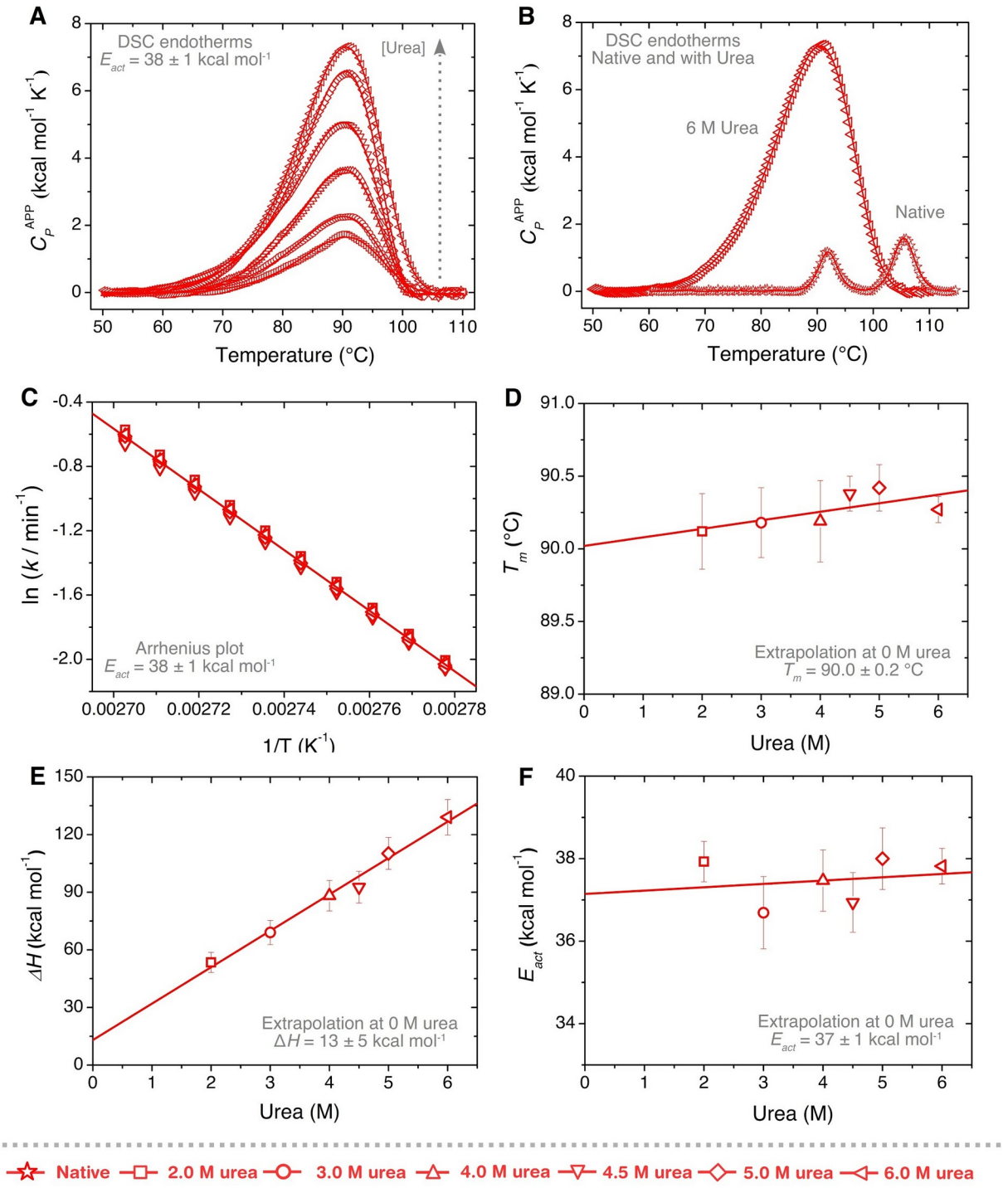

Fig. S10. Irreversible thermal unfolding of DeNovoTIM14 in the presence of urea. **A)** DSC endotherms at different urea concentrations (2.0 to 6.0 M). Lines represent the best fit to a two-state irreversible model. **B)** Comparison between DeNovoTIM14 endotherms in native conditions and at 6.0 M urea. **C)** Arrhenius plot. The line shows the best fit to the Arrhenius equation (R^2: 0.99). **D)** T_m vs. urea concentration (R^2: 0.70). **E)** ΔH vs. urea concentration (R^2: 0.99). **F)** E_{act} vs. urea concentration (R^2: 0.62). In all experiments protein concentration was 1 mg mL^{-1} in 10 mM sodium phosphate pH 8.

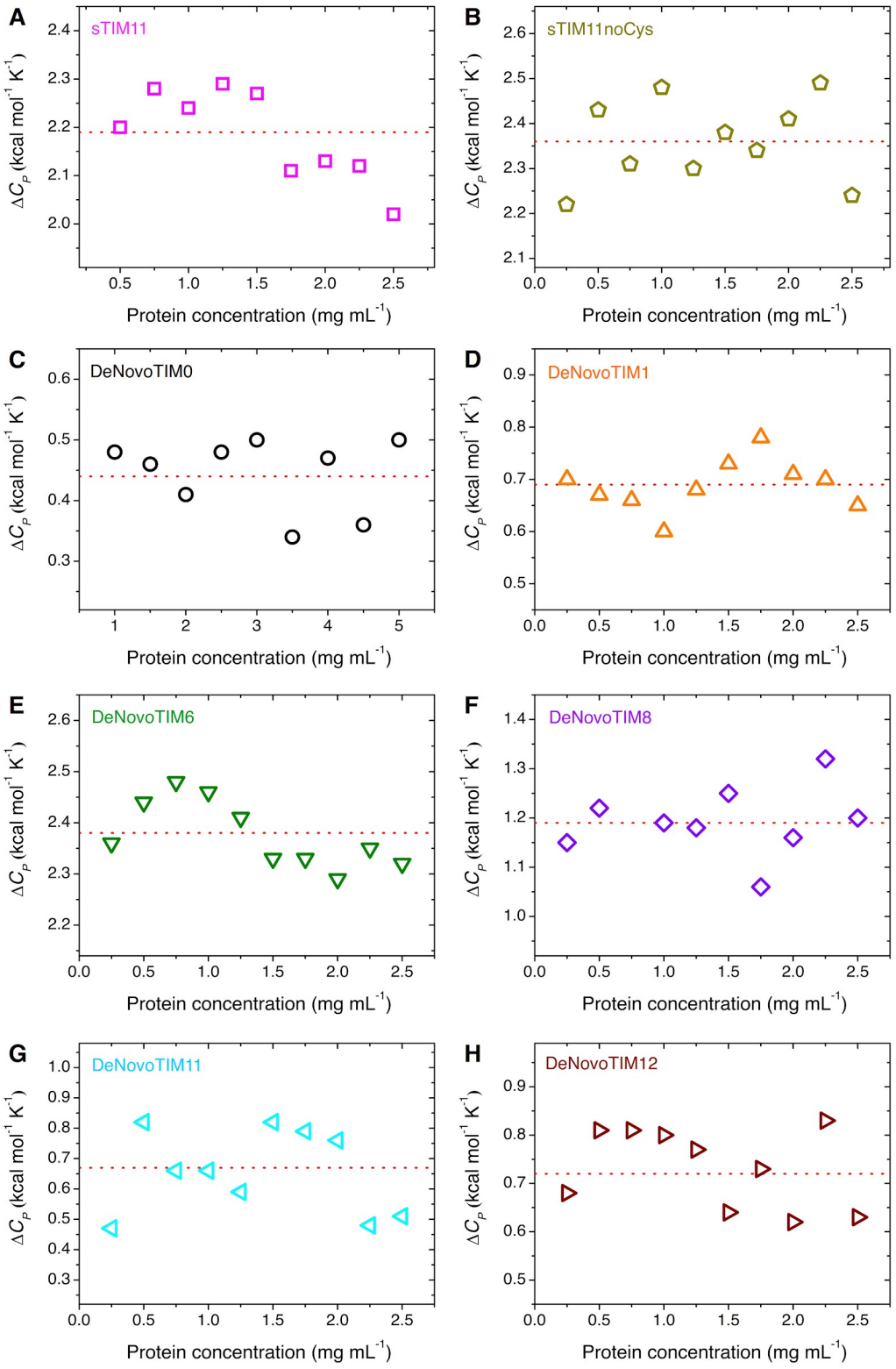

Fig. S11. ΔC_P determination of DeNovoTIMs at different protein concentrations. DSC experiments (Fig. S8) were carried out in the range of 0.25-2.5 mg mL^{-1} (panels **A**, **B**, **D**, **E**, **F**, **G**, **H**) or 1.0-5.0 mg mL^{-1} (panel **C**). Dotted red lines represent the average value for each protein.

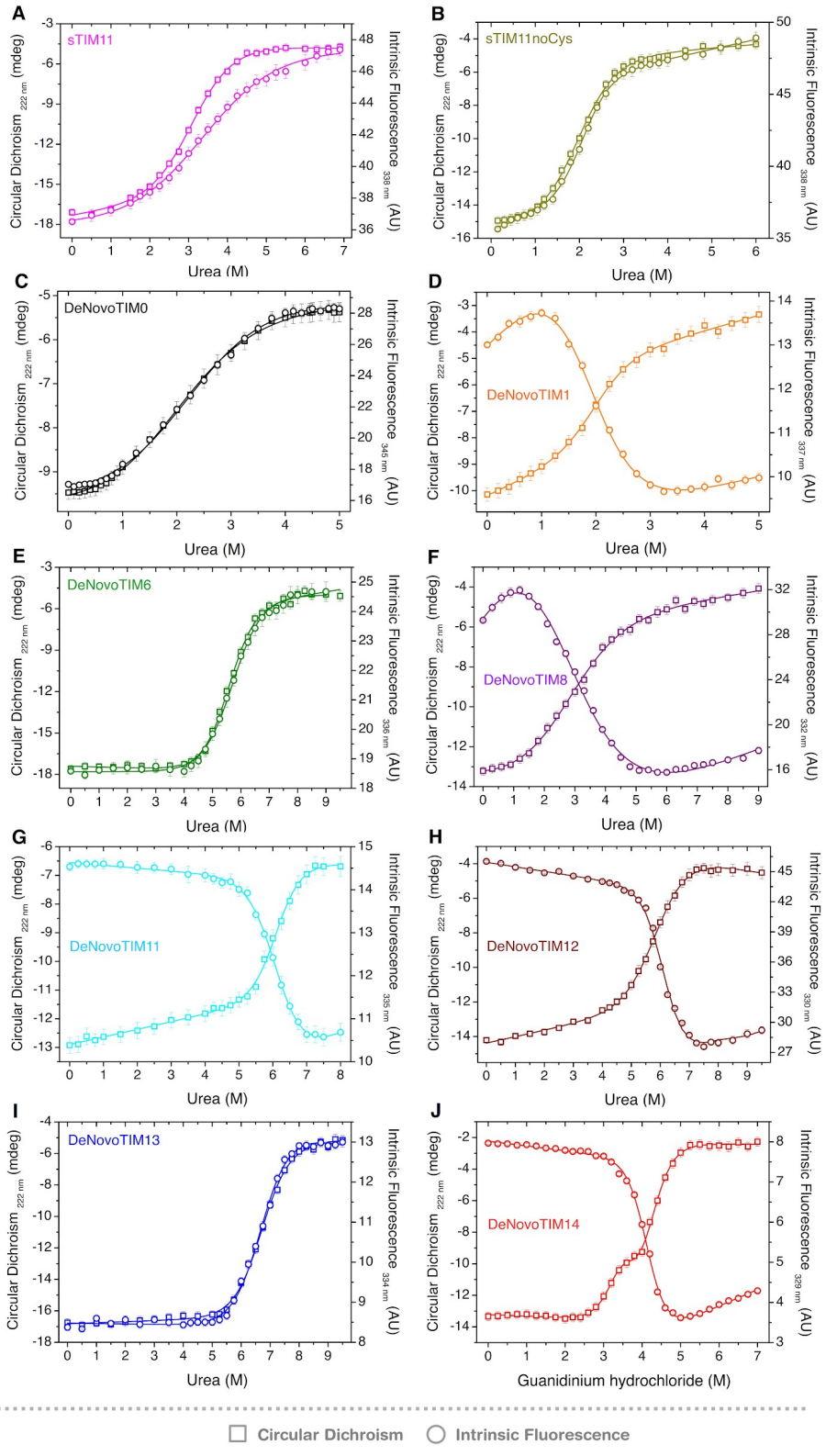

Fig. S12. Chemical unfolding of DeNovoTIMs followed by CD and IF (raw data). Lines are the best fits to a two-state model, except for DeNovoTIM14 where a three-state model was used. In all experiments protein concentration was 0.1 mg mL^{-1} in 10 mM sodium phosphate pH 8.

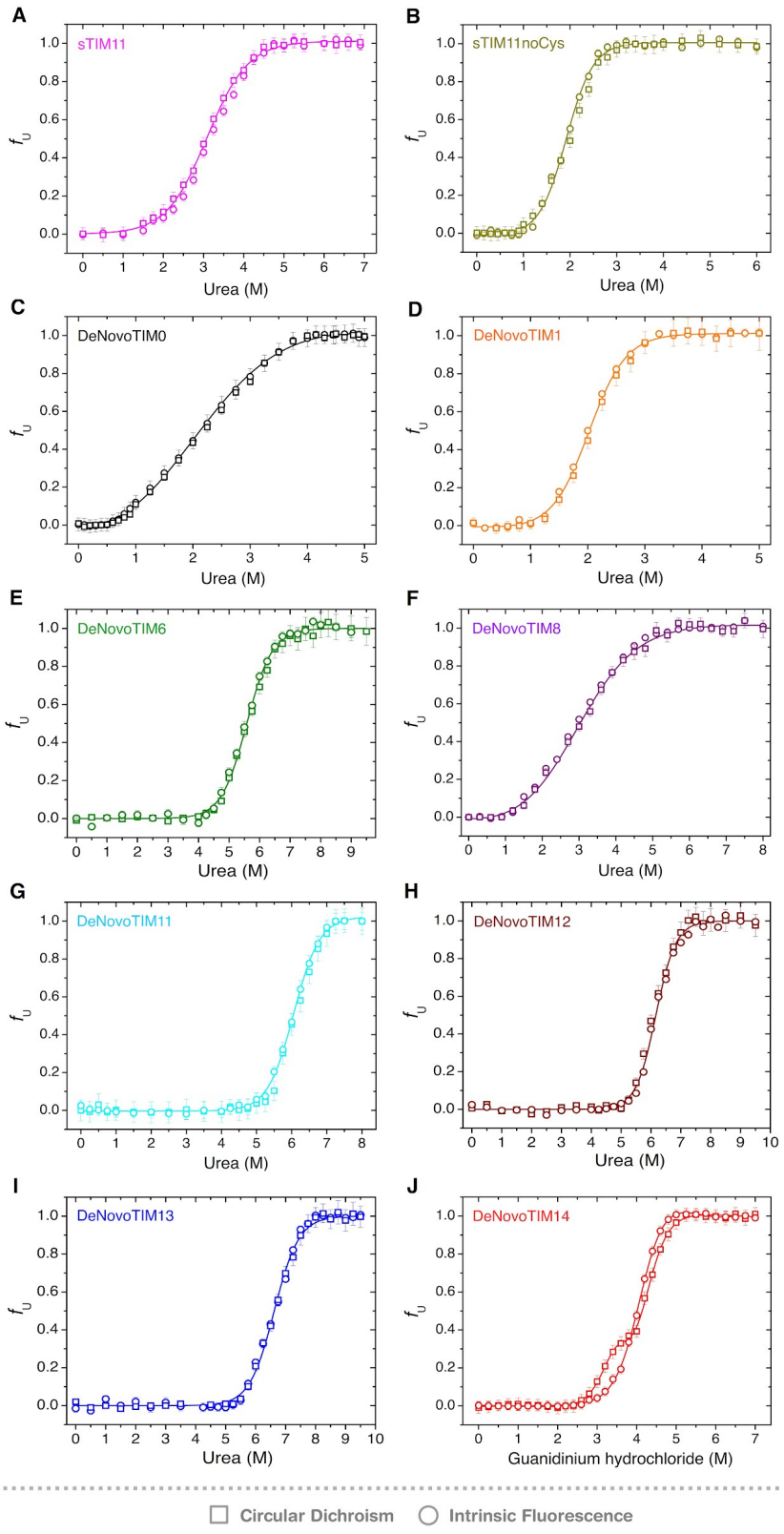

Fig. S13. Chemical unfolding of DeNovoTIMs followed by CD and IF (normalized data). Lines are the best fits to a two-state model, except for DeNovoTIM14 where a three-state model was used. In all experiments protein concentration was 0.1 mg mL^{-1} in 10 mM sodium phosphate pH 8.

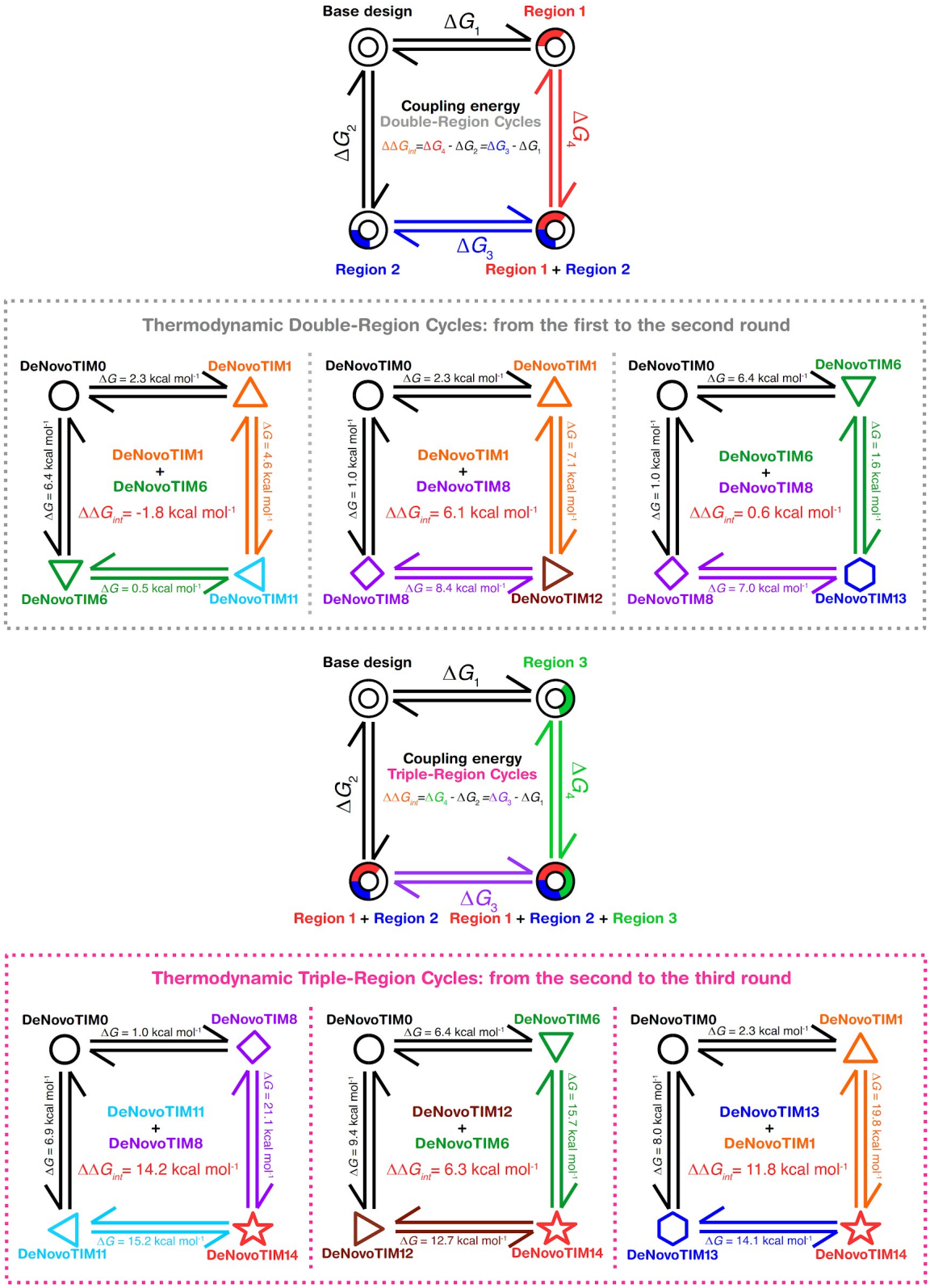

Fig. S14. Thermodynamic cycles for DeNovoTIMs. Thermodynamic cycles for double- and triple-region designs (top and bottom panels, respectively). Coupling energy ($\Delta\Delta G_{int}$) for each case is shown inside each cycle.

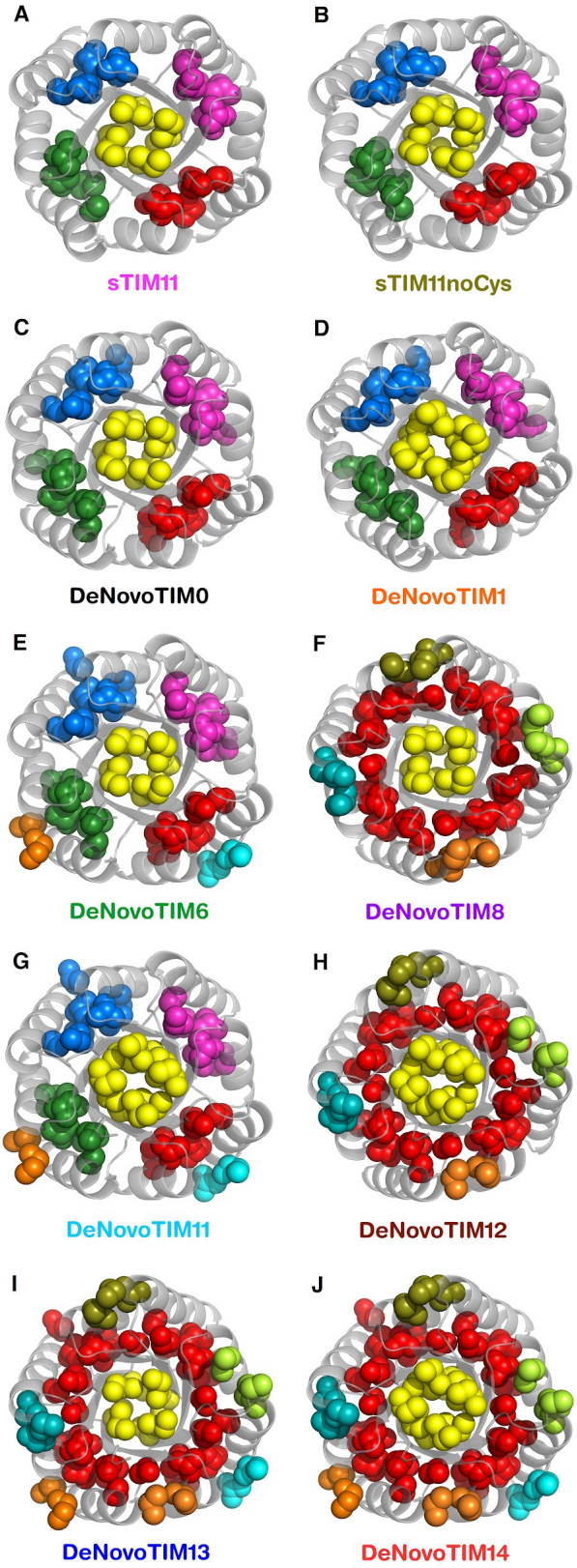

Fig. S15. Hydrophobic clusters of DeNovoTIMs. Clusters are shown in different colors. Hydrophobic clusters properties are reported in table S7.

Supplementary Tables

List of supplementary tables

- **Table S1:** Amino acid sequences of DeNovoTIM collection.
- **Table S2**: List of mutations in DeNovoTIM collection.
- **Table S3**: Aromatic residues in DeNovoTIM collection.
- **Table S4**: Sequence identity matrix of DeNovoTIM collection.
- **Table S5**: Biochemical and biophysical characterization of the DeNovoTIM collection.
- **Table S6**: Crystallographic data collection and refinement statistics for the three-dimensional structures.
- **Table S7**: Comparison of structural features between Rosetta models and three-dimensional structures.

Table S1. Amino acid sequences of DeNovoTIM collection.

***de novo* TIM barrel**	**Sequence**
sTIM11	DKDEAWKCVEQLRREGATQIAYRSDDWRDLKEAWKKGADILIVDATDKDEAWKQVEQLRREGATQIAYRSDDWRDLKEAWKKGADILIVDAT DKDEAWKQVEQLRREGATQIAYRSDDWRDLKEAWKKGADILIVDATDKDEAWKQVEQLRREGATQIAYRSDDWRDLKEAWKKGADILICDAT
sTIM11noCys	DKDEAWKQVEQLRREGATQIAYRSDDWRDLKEAWKKGADILIVDATDKDEAWKQVEQLRREGATQIAYRSDDWRDLKEAWKKGADILIVDAT DKDEAWKQVEQLRREGATQIAYRSDDWRDLKEAWKKGADILIVDATDKDEAWKQVEQLRREGATQIAYRSDDWRDLKEAWKKGADILIVDAT
DeNovoTIM0	DKDEAWKQVEQLRREGATQIAYRSDDWRDLKEAVKKGGDILIVDATDKDEAWKQVEQLRREGATQIAYRSDDWRDLKEAVKKGGDILIVDAT DKDEAWKQVEQLRREGATQIAYRSDDWRDLKEAVKKGGDILIVDATDKDEAWKQVEQLRREGATQIAYRSDDWRDLKEAVKKGGDILIVDAT
DeNovoTIM1	DKDEAWKQVEQLRREGATQIVYISDDWRDLKEAVKKGGDILIVDATDKDEAWKQVEQLRREGATQIWYISDDWRDLKEAVKKGGDVLIVDAT DKDEAWKQVEQLRREGATQIVYISDDWRDLKEAVKKGGDILIVDATDKDEAWKQVEQLRREGATQIWYISDDWRDLKEAVKKGGDVLIVDAT
DeNovoTIM2	DKDEAWKQVEQLRREGATQIVYQSDDWRDLKEAVKKGGDILMVDATDKDEAWKQVEQLRREGATQIMYISDDWRDLKEAVKKGGDFLVVDAT DKDEAWKQVEQLRREGATQIVYQSDDWRDLKEAVKKGGDILMVDATDKDEAWKQVEQLRREGATQIMYISDDWRDLKEAVKKGGDFLVVDAT
DeNovoTIM3	DKDEAWKQVEQLRREGATQIMYVSDDWRDLKEAVKKGGDSLLVDATDKDEAWKQVEQLRREGATQILYKSDDWRDLKEAVKKGGDTLVVDAT DKDEAWKQVEQLRREGATQIMYVSDDWRDLKEAVKKGGDSLLVDATDKDEAWKQVEQLRREGATQILYKSDDWRDLKEAVKKGGDTLVVDAT
DeNovoTIM4	DKDEAWKQVEQLRREGATQIMYFSDDWRDLKEAVKKGGDLLVVDATDKDEAWKQVEQLRREGATQILYISDDWRDLKEAVKKGGDILLVDAT DKDEAWKQVEQLRREGATQIMYFSDDWRDLKEAVKKGGDLLVVDATDKDEAWKQVEQLRREGATQILYISDDWRDLKEAVKKGGDILLVDAT
DeNovoTIM5	DKDEAWKQVEQLRRLGATQIAYRSDDWRDLREAVKKGGDILIVDATDKDEAWKQVEQLRRLGATQIAYRSDDWRDLREAVKKGGDILIVDAT DKDEAWKQVEQLRRLGATQIAYRSDDWRDLREAVKKGGDILIVDATDKDEAWKQVEQLRRLGATQIAYRSDDWRDLREAVKKGGDILIVDAT
DeNovoTIM6	DKDEAWKQVEILRRLGAKQIAYRSDDWRDLQEALKKGGDILIVDATDKDEAWKQVEILRRLGAKQIAYRSDDWRDLQEALKKGGDILIVDAT DKDEAWKQVEILRRLGAKQIAYRSDDWRDLQEALKKGGDILIVDATDKDEAWKQVEILRRLGAKQIAYRSDDWRDLQEALKKGGDILIVDAT
DeNovoTIM7	DKDEAWKQVEILRRLGAKQIAYRSDDWRDLDEARKKGGDILIVDATDKDEAWKQVEILRRLGAKQIAYRSDDWRDLDEARKKGGDILIVDAT DKDEAWKQVEILRRLGAKQIAYRSDDWRDLDEARKKGGDILIVDATDKDEAWKQVEILRRLGAKQIAYRSDDWRDLDEARKKGGDILIVDAT
DeNovoTIM8	DVDEMLKQVEQLRREGATQIAVRSDDWRILKEAVKKGGDILIVDATDVDEMLKQVEQLRREGATQIAVRSDDWRILKEAVKKGGDILIVDAT DVDEMLKQVEQLRREGATQIAVRSDDWRILKEAVKKGGDILIVDATDVDEMLKQVEQLRREGATQIAVRSDDWRILKEAVKKGGDILIVDAT
DeNovoTIM9	DPDEAQKQVEQLRREGATQIAIRSDDWRYLKEAVKKGGDILIVDATDPDEAQKQVEQLRREGATQIAIRSDDWRYLKEAVKKGGDILIVDAT DPDEAQKQVEQLRREGATQIAIRSDDWRYLKEAVKKGGDILIVDATDPDEAQKQVEQLRREGATQIAIRSDDWRYLKEAVKKGGDILIVDAT
DeNovoTIM10	DSDEAIKQVEQLRREGATQIAVRMDDWRKLKEAVKKGGDILIVDATDSDEAIKQVEQLRREGATQIAVRMDDWRKLKEAVKKGGDILIVDAT DSDEAIKQVEQLRREGATQIAVRMDDWRKLKEAVKKGGDILIVDATDSDEAIKQVEQLRREGATQIAVRMDDWRKLKEAVKKGGDILIVDAT
DeNovoTIM11	DKDEAWKQVEILRRLGAKQIVYISDDWRDLQEALKKGGDILIVDATDKDEAWKQVEILRRLGAKQIWYISDDWRDLQEALKKGGDVLIVDAT DKDEAWKQVEILRRLGAKQIVYISDDWRDLQEALKKGGDILIVDATDKDEAWKQVEILRRLGAKQIWYISDDWRDLQEALKKGGDVLIVDAT
DeNovoTIM12	DVDEMLKQVEQLRREGATQIVVISDDWRILKEAVKKGGDILIVDATDVDEMLKQVEQLRREGATQIWVISDDWRILKEAVKKGGDVLIVDAT DVDEMLKQVEQLRREGATQIVVISDDWRILKEAVKKGGDILIVDATDVDEMLKQVEQLRREGATQIWVISDDWRILKEAVKKGGDVLIVDAT
DeNovoTIM13	DVDEMLKQVEILRRLGAKQIAVRSDDWRILQEALKKGGDILIVDATDVDEMLKQVEILRRLGAKQIAVRSDDWRILQEALKKGGDILIVDAT DVDEMLKQVEILRRLGAKQIAVRSDDWRILQEALKKGGDILIVDATDVDEMLKQVEILRRLGAKQIAVRSDDWRILQEALKKGGDILIVDAT
DeNovoTIM14	DVDEMLKQVEILRRLGAKQIVVISDDWRILQEALKKGGDILIVDATDVDEMLKQVEILRRLGAKQIWVISDDWRILQEALKKGGDVLIVDAT DVDEMLKQVEILRRLGAKQIVVISDDWRILQEALKKGGDILIVDATDVDEMLKQVEILRRLGAKQIWVISDDWRILQEALKKGGDVLIVDAT

Table S2. List of mutations in DeNovoTIM collection.

de novo TIM barrel	Symmetry (fold)	Number of mutations in each modular unit[a]	Total number of mutations in the Sequence	Mutations added in each modular unit[a]
sTIM11	pseudo 4	-----	-----	-----
sTIM11noCys	4	2 (non-symmetric)	2	C8Q, C181V
DeNovoTIM0	4	2	8	W34V, A38G
DeNovoTIM1	2	5	10	A21V, R23I, A67W, R69I, I86V
DeNovoTIM2	2	7	14	A21V, R23Q, I42M, A67M, R69I, I86F, I88V
DeNovoTIM3	2	8	16	A21M, R23V, I40S, I42L, A67L, R69K, I86T, I88V
DeNovoTIM4	2	7	14	A21M, R23F, I40L, I42V, A67L, R69I, I88L
DeNovoTIM5	4	2	8	E15L, K31R
DeNovoTIM6	4	5	20	Q11I, E15L, T18K, K31Q, V34L
DeNovoTIM7	4	5	20	Q11I, E15L, T18K, K31D, V34R
DeNovoTIM8	4	5	20	K2V, A5M, W6L, Y22V, D29I
DeNovoTIM9	4	4	16	K2P, W6Q, Y22I, D29Y
DeNovoTIM10	4	5	20	K2S, W6I, Y22V, S24M, D29K
DeNovoTIM11	2	15	30	Q11I, E15L, T18K, A21V, R23I, K31Q, V34L, Q57I, E61L, A67W, T64K, R69I, K77Q, V80L, I86V
DeNovoTIM12	2	15	30	K2V, A5M, W6L, A21V, Y22V, R23I, D29I, K48V, A51M, W52L, A67W, Y68V, R69I, D75I, I86V
DeNovoTIM13	4	10	40	K2V, A5M, W6L, Q11I, E15L, T18K, Y22V, D29I, K31Q, V34L
DeNovoTIM14	2	25	50	K2V, A5M, W6L, Q11I, E15L, T18K, A21V, Y22V, R23I, D29I, K31Q, V34L, K48V, A51M, W52L, Q57I, E61L, T64K, A67W, Y68V, R69I, D75I, K77Q, V80L, I86V

[a] Only the mutations incorporated in each design are shown. See Fig. S2 for the complete sequence alignment.

Table S3. Aromatic residues in DeNovoTIM collection.

de novo TIM barrel	Number of Tyr residues in each modular unit	Total number of Trp residues	Position of Trp residues in the modular unit	Number of Tyr residues in each modular unit	Total number of Tyr residues	Position of Tyr residues in the modular unit
sTIM11	3	12	W6, W27, W34	1	4	Y22
sTIM11noCys	3	12	W6, W27, W34	1	4	Y22
DeNovoTIM0	2	8	W6, W27	1	4	Y22
DeNovoTIM1	5	10	W6, W27, W52, W67, W73	2	4	Y22, Y68
DeNovoTIM2	4	8	W6, W27, W52, W73	2	4	Y22, Y68
DeNovoTIM3	4	8	W6, W27, W52, W74	2	4	Y22, Y68
DeNovoTIM4	4	8	W6, W27, W52, W75	2	4	Y22, Y68
DeNovoTIM5	2	8	W6, W27	1	4	Y22
DeNovoTIM6	2	8	W6, W27	1	4	Y22
DeNovoTIM7	2	8	W6, W27	1	4	Y22
DeNovoTIM8	1	4	W27	0	0	-----
DeNovoTIM9	1	4	W27	0	0	-----
DeNovoTIM10	1	4	W27	0	0	-----
DeNovoTIM11	5	10	W6, W27, W52, W67, W73	2	4	Y22, Y68
DeNovoTIM12	5	10	W6, W27, W52, W67, W73	0	0	-----
DeNovoTIM13	2	8	W6, W27	0	0	-----
DeNovoTIM14	5	10	W6, W27, W52, W67, W73	0	0	-----

Table S4. Sequence identity matrix of DeNovoTIM collection.

	sTIM11	sTIM11noCys	DeNovoTIM0	DeNovoTIM1	DeNovoTIM2	DeNovoTIM3	DeNovoTIM4	DeNovoTIM5	DeNovoTIM6	DeNovoTIM7	DeNovoTIM8	DeNovoTIM9	DeNovoTIM10	DeNovoTIM11	DeNovoTIM12	DeNovoTIM13	DeNovoTIM14
sTIM11																	
sTIM11noCys	99																
DeNovoTIM0	95	96															
DeNovoTIM1	89	90	95														
DeNovoTIM2	87	88	92	95													
DeNovoTIM3	86	87	91	91	92												
DeNovoTIM4	87	88	92	92	92	94											
DeNovoTIM5	90	91	96	90	88	87	88										
DeNovoTIM6	86	87	89	84	82	80	82	91									
DeNovoTIM7	86	87	89	84	82	80	82	91	96								
DeNovoTIM8	84	85	89	84	82	80	82	85	78	78							
DeNovoTIM9	86	87	91	86	84	83	84	87	80	80	89						
DeNovoTIM10	84	85	89	84	82	80	82	85	78	78	89	89					
DeNovoTIM11	80	82	84	89	84	80	82	86	95	90	73	75	73				
DeNovoTIM12	78	79	84	89	84	80	82	79	73	73	95	84	84	78			
DeNovoTIM13	75	76	78	73	71	70	71	80	89	85	89	78	78	84	84		
DeNovoTIM14	70	71	73	78	73	70	71	75	84	79	84	73	73	89	89	95	

Table S5. Biochemical and biophysical characterization of DeNovoTIM collection.

de novo TIM barrel	Expression/Solubility properties		Spectroscopic properties										Hydrodynamic properties[e]				
			Circular Dichroism			Intrinsic Fluorescence[d]											
			Predicted secondary structure content (%)[c]														
	Soluble overexpression[a]	Aggregation-prone[b]	α-helix	β-strand	Random coil	Native λ_{max} (nm)	Unfolded λ_{max} (nm)	$\Delta\lambda_{max\ N-U}$ (nm)	Native SCM (nm)	Unfolded SCM (nm)	ΔSCM_{N-U} (nm)		Theoretical MW (Da)	Experimental MW (Da)	Exp./ Theor. ratio	Oligomeric state	Stokes radius (Å)
sTIM11	+++	+	46.3 (46.0)	19.8 (20.0)	34.0 (34.0)	338	350	12	354	360	7		22854	22017 ± 465	1.0	Monomer	23.2 ± 0.5
sTIM11noCys	+++	+	47.6 (48.1)	19.2 (22.8)	33.2 (29.1)	338	349	11	353	361	7		22875	20670 ± 146	0.9	Monomer	22.6 ± 0.1
DeNovoTIM0	++	+	41.4	30.7	27.9	345	352	7	357	362	5		22471	29827 ± 309	1.3	Monomer	26.1 ± 0.3
DeNovoTIM1	++	++	42.7	29.3	27.9	337	350	13	354	360	6		22557	21017 ± 637	0.9	Monomer	22.8 ± 0.8
DeNovoTIM6	+++	+	46.5 (43.4)	18.8 (20.7)	34.8 (35.9)	336	350	14	352	361	9		22568	22000 ± 440	1.0	Monomer	23.2 ± 0.5
DeNovoTIM8	++	++	47.1	22.3	30.6	332	351	19	348	361	13		22039	20518 ± 360	0.9	Monomer	22.6 ± 0.3
DeNovoTIM11	+	+++	46.9	22.9	30.0	335	349	14	353	362	9		22598	20920 ± 572	0.9	Monomer	22.3 ± 0.6
DeNovoTIM12	+++	+	45.5	24.7	29.7	330	351	21	347	360	13		22125	20029 ± 760	0.9	Monomer	23.1 ± 0.9
DeNovoTIM13	+++	+++	48.3 (48.8)	18.1 (21.8)	33.5 (29.4)	334	351	17	351	360	8		22080	21601 ± 725	1.0	Monomer	22.7 ± 0.7
DeNovoTIM14	+	+++	50.3	18.7	31.1	329	350 (331)	21	346	362 (349)	15		22166	25357 ± 1833	1.2	Monomer	24.7 ± 1.8

[a] Symbols represent the amount of protein purified from the soluble fraction: +++ >10 mg L^{-1} culture, ++ 5-10 mg L^{-1} culture, + 2-5 mg L^{-1} culture.

[b] Symbols represent the protein propensity to aggregate: +++ aggregation visible within the first week after purification, ++ aggregation visible between 1-2 weeks after purification, + not visible aggregation after at least 1 month after purification.

[c] numbers within brackets are the calculated value from the three-dimensional structure.

[d] unfolded state represents the spectra at 9.0 M urea.

[e] ± indicates the standard deviation calculated from 4 different experiments at protein concentrations of 0.01, 0.5, 1.0, and 2.0 mg mL^{-1}.

Table S6. Crystallographic data collection and refinement statistics for the three-dimensional structures.

***de novo* TIM barrel**	**sTIM11noCys**	**DeNovoTIM6**	**DeNovoTIM13**
Data collection[a]			
PDB ID	6YQY	6Z2I	6YQX
Crystallization condition	0.2 M Ammonium sulfate 0.1 M Trisodium citrate pH: 5.6 25% w/v PEG 4000	0.095 M Sodium citrate pH: 5.0 19% v/v Isopropanol 25% w/v PEG 4000 5% v/v Glycerol	0.17 M Sodium acetate 0.085 M TRIS pH: 8.5 25.5% w/v PEG 4000 15% v/v Glycerol
Resolution range (Å)	47.15 – 1.88 (1.94 – 1.88)	30.93 – 2.90 (3.01 – 2.90)	44.79 – 1.64 (1.70 – 1.64)
Space group	P 4_1 2_1 2 (92)	P 4 (75)	P 3_2 (145)
Unit cell dimensions			
a, b, c, (Å)	50.45, 50.45, 132.41	87.48, 87.48, 44.26	51.72, 51.72, 63.97
α, β, γ (°)	90, 90, 90	90, 90, 90	90, 90, 120
Total reflections	342791 (32681)	56016 (3033)	79664 (7327)
Unique reflections	14703 (1410)	7620 (389)	23407 (2280)
Multiplicity	23.3 (23.2)	7.4 (7.8)	3.4 (3.2)
Completeness (%)	99.9 (99.0)	99.8 (100.0)	99.5 (97.6)
Mean I / sigma (I)	27.0 (1.9)	4.3 (1.0)	14.3 (1.5)
R-merge	0.061 (1.281)	0.180 (1.195)	0.042 (0.552)
CC1/2	1.000 (0.810)	0.940 (0.773)	0.998 (0.659)
Average mosaicity (deg)	0.109	0.179	0.116
Refinement statistics[a]			
R_{work} , R_{free}	0.220 (0.287), 0.271 (0.371)	0.316 (0.368), 0.372 (0.431)	0.171 (0.274), 0.201 (0.329)
Average B-value (Å^2)	54.2	89.3	39.1
Protein	53.9	89.4	37.7
Ligand	-----	-----	61.3
Solvent	62.2	77.1	53.5
Overall B factor from Wilson Plot (Å^2)	41.0	73.8	28.4
Number of atoms	1489	1185	1603
Protein	1440	1175	1464
Ligand	0	0	7
Water	49	10	132
Protein residues	178	168	181
RMS (bonds) (Å)	0.008	0.003	0.006
RMS (angles) (°)	0.900	0.560	0.770
Ramachandran favored (%)	97.1	93.6	100.0
Ramachandran allowed (%)	2.9	6.4	0.0
Ramachandran outliers (%)	0.0	0.0	0.0
Rotamer outliers (%)	0.0	0.0	0.0
Clashscore	8.2	5.3	3.9

[a] Statistics for the highest resolution shell are shown in parentheses.

Table S7. Comparison of structural features between Rosetta models and three-dimensional structures.

Design round	Base designs					First-round designs: Internal Core				First-round designs: Bottom Core				First-round designs: Top Core			Second-round designs				Third-round design
Property / *de novo* TIM barrel	sTIM11		sTIM11noCys		DeNovoTIM0	DeNovoTIM1	DeNovoTIM2	DeNovoTIM3	DeNovoTIM4	DeNovoTIM5	DeNovoTIM6		DeNovoTIM7	DeNovoTIM8	DeNovoTIM9	DeNovoTIM10	DeNovoTIM11	DeNovoTIM12	DeNovoTIM13		DeNovoTIM14
	model	structure	model	structure	model	model	model	model	model	model	model	structure	model	model	model	model	model	model	model	structure	model
Structural properties																					
H-bonds	236	204	194	171	198	201	197	201	201	209	176	138	189	201	184	177	169	174	167	195	163
Salt bridges	47	22	37	16	27	39	39	41	39	47	27	4	37	35	25	27	34	14	22	18	28
Total area in hydrophopic clusters (Å^2)	4088	3765	4260	4215	4793	6530	4800	4774	6042	5221	5195	5097	4533	6849	5812	5507	4485	7471	6381	6148	7730
Area of the major hydrophopic cluster (Å^2)	1171	1116	1035	1111	1066	2605	983	984	2114	1169	1180	1111	1162	4610	4611	4329	2524	4265	4416	4351	4519
% of total area present in the major hydrophopic cluster	29	30	24	26	22	40	20	21	35	22	23	22	26	67	79	79	56	57	69	71	58
Total residues in hydrophobic clusters	31	31	32	32	36	42	36	36	40	40	41	43	36	52	40	40	50	57	56	60	64
Residues in the major hydrophobic cluster	8	8	8	8	8	14	7	7	12	8	8	9	8	32	32	32	14	32	33	38	34
% of total residues present in the major hydrophobic cluster	26	26	25	25	22	33	19	19	30	20	20	21	22	62	80	80	28	56	59	63	53
Total contacts in hydrophobic clusters	82	81	89	91	98	120	84	88	112	104	103	113	94	143	122	114	129	152	133	150	166
Contacts in the major hydrophobic cluster	24	23	24	23	23	48	18	18	40	24	23	24	23	96	99	92	48	91	94	111	104
% of total contacts present in the major hydrophobic cluster	29	28	27	25	23	40	21	20	36	23	22	21	24	67	81	81	37	60	71	74	63
Total ASA of the folded protein (Å^2)	8661	8669	8784	8761	8920	8336	8366	8362	8360	8323	9126	9052	9149	8472	9187	9140	9002	9016	9070	8867	8730
Hydrophobic ASA of the folded protein (%)	48	51	46	51	47	46	45	46	46	47	52	58	50	46	48	48	50	50	53	53	51
Total ΔASA buried on protein folding (Å^2)	18893	17815	18844	17331	18199	19380	19335	19017	19429	19060	18878	17251	18141	18955	18000	17947	19469	19008	19111	18928	20048
Hydrophobic ΔASA buried on protein folding (%)	79	77	79	74	77	79	78	78	79	79	79	70	81	80	78	80	77	80	79	75	78
Physicochemical amino acid properties (%)																					
Aliphatic (AGILPV)	34		35		37	38	35	35	37	39	41		39	43	41	41	42	45	48		49
Aromatic (FHWY)	9		9		7	8	8	7	8	7	7		7	2	4	2	8	3	2		3
Charged (DEHKR)	43		43		43	41	41	42	41	41	41		46	39	39	41	39	37	37		35
Hydrophobic (CFILMVW)	24		24		24	28	27	25	28	26	28		26	33	24	28	33	37	37		41
Polar (DEKNQR)	49		50		50	48	49	49	48	48	48		50	46	48	48	46	43	43		41